RESEARCH ARTICLE

Epileptic Seizure Detection Using a Recurrent Neural Network With Temporal Features Derived From a Scale Mixture EEG Model

AKIRA FURUI [ID]**1, (Member, IEEE), RYOTA ONISHI2, TOMOYUKI AKIYAMA** [ID]**3,
AND TOSHIO TSUJI** [ID]**1, (Life Member, IEEE)**

[1]Graduate School of Advanced Science and Engineering, Hiroshima University, Higashihiroshima 739-8527, Japan
[2]Graduate School of Engineering, Hiroshima University, Higashihiroshima 739-8527, Japan
[3]Department of Pediatric Neurology, Okayama University Hospital, Okayama 700-8558, Japan

Corresponding authors: Akira Furui (akirafurui@hiroshima-u.ac.jp) and Toshio Tsuji (toshiotsuji@hiroshima-u.ac.jp)

ABSTRACT Automated detection of epileptic seizures from scalp Electroencephalogram (EEG) is crucial for improving epilepsy diagnosis and management. This paper presents an automated inter-patient epileptic seizure detection method using multichannel EEG signals. The proposed method uses a scale mixture-based stochastic EEG model for feature extraction and a recurrent neural network for seizure detection. Specifically, the stochastic model, which accounts for uncertainties in EEG amplitude, is fitted to a specific frequency band to extract relevant seizure features. Then, a recurrent neural network-based recognition architecture learns the temporal evolution of these features. We evaluated our method using EEG data from 20 patients with focal epilepsy and conducted comprehensive assessments, including ablation studies on classifiers and features. Our results demonstrate that our approach outperforms static classifiers and existing feature sets, achieving high sensitivity while maintaining acceptable specificity. Furthermore, our feature set showed efficacy both independently and as a complement to existing features, indicating its robustness in seizure detection tasks. These findings reveal that learning the temporal evolution of the stochastic fluctuation and amplitude information of EEG extracted using a stochastic model enables highly accurate seizure detection, potentially advancing automated epilepsy diagnosis in clinical settings.

INDEX TERMS Electroencephalogram (EEG), stochastic model, scale mixture model, epileptic seizure detection, non-Gaussianity, recurrent neural network.

I. INTRODUCTION

Epilepsy is a common neurological disease that affects approximately 50 million people worldwide [1], [2]. This disease is diagnosed after the occurrence of at least one unprovoked, transient, abnormal neuronal activity in the brain, called an epileptic seizure [3]. Electroencephalogram (EEG) is one of the most important tools in the diagnosis of epileptic seizures because it is non-invasive and relatively easy to record. EEG records electrical activity generated by groups of neurons from the scalp surface and can extract and

The associate editor coordinating the review of this manuscript and approving it for publication was Md Kafiul Islam [ID].

observe various features related to brain activity. In particular, during epileptic seizures, EEG signals exhibit abnormal waveforms, such as rhythmic activities and repetitive spikes with spatial and temporal evolution.

Despite the importance of EEG in epilepsy diagnosis, the current method of detecting epileptic seizures through visual inspection by doctors has several limitations. It requires long observation periods and expertise, and diagnoses may differ across specialists due to the subjectivity of EEG interpretation. Moreover, it is time-consuming and labor-intensive, especially for long-term EEG recordings. These limitations highlight the need for an automated and quantitative method for epileptic seizure detection. Accurate and automated

seizure detection is important both for recording seizure history and alerting medical workers, and for developing vagus nerve stimulators and drug-release devices with the potential to reduce the severity of epileptic seizures [4].

Two main approaches have been developed for epileptic seizure detection: patient-specific classification [4], [5], [6], [7], [8] and inter-patient classification [9], [10], [11], [12]. While the patient-specific approach can achieve high accuracy by accounting for individual characteristics, it requires generating individual classification models for each patient, which may not be feasible in clinical and emergency settings [13], [14]. On the other hand, the inter-patient approach aims to detect seizures in any patient, making it more suitable for clinical use [10]. However, this approach faces challenges in accounting for features common to different individuals while maintaining high generalization performance.

Recent efforts in inter-patient seizure detection have focused on feature extraction from EEG signals. Various techniques have shown effectiveness, including time-domain features [15], [16], [17], [18] and frequency domain features [19], [20], [21]. However, while these methods have shown success in capturing various aspects of EEG signals, there remains a challenge in fully representing the complex, non-Gaussian nature of EEG signals [22], [23], [24] during seizures. This presents an opportunity to explore new approaches that may provide additional insights into these signal characteristics.

To contribute to this ongoing research and address the challenge of capturing non-Gaussian properties, we previously introduced an approach to feature extraction for seizure detection based on a Scale Mixture Model (SMM) of EEG [23]. This model assumes that the non-Gaussianity of EEG signals arises from the stochastic fluctuations of their variance, which manifests as subtle amplitude variations leading to heavier tails in the signal distribution. By formulating this structure in a stochastic model with variable Gaussianity, we can compute non-Gaussianity features that reflect amplitude fluctuations. Our statistical analysis demonstrated that the parameters derived from the SMM showed a stronger correlation with epileptic seizures compared to conventional features, suggesting their potential effectiveness in seizure detection. However, the effectiveness of this approach in detecting seizures for unseen patients had not yet been demonstrated in a practical setting.

Building upon these findings, in this paper, we propose an automatic epileptic seizure detection method based on a Recurrent Neural Network (RNN) with temporal features derived from the SMM of EEG. We utilize the SMM parameters as features, capturing the non-Gaussian characteristics and amplitude information of EEG signals in a unified framework, and employ an RNN to model the temporal dynamics of these features.

The main contributions of this study are as follows:
- Comprehensive feature extraction using a scale mixture-based stochastic model that captures both

non-Gaussianity and amplitude information of EEG signals during seizures.
- Temporal dynamics modeling through an RNN for seizure detection, enabling the analysis of time-series changes in the extracted features.
- Extensive ablation studies to validate the contribution of our proposed features and classification models, comparing them with existing feature extraction methods and classifier architectures.

By focusing on the unique non-Gaussian nature of EEG signals during seizures, our approach has the potential to detect subtle changes in EEG patterns. Additionally, we aim to contribute to ongoing efforts to improve the accuracy and generalizability of epileptic seizure detection among patients by integrating SMM-based features specific to non-Gaussian characteristics with conventional features and by leveraging the temporal modeling capabilities of RNNs.

The remainder of this paper is organized as follows: Section II reviews related work; Section III outlines the proposed epileptic seizure detection method; Section IV details the experimental setup; Section V presents the results; Section VI discusses the findings; and Section VII concludes the paper.

II. RELATED WORK
A. EEG-BASED EPILEPTIC SEIZURE DETECTION
1) EEG FEATURE EXTRACTION
Feature extraction plays an important role in epileptic seizure detection from EEG signals. Various approaches have been proposed to address this challenge. Time-domain features, such as amplitude-based measures, entropy, and higher-order statistics, have been widely used due to their simplicity and interpretability [15], [16], [17], [18]. Frequency-domain features, including band-specific power, spectral characteristics, and wavelet features, have also shown effectiveness in capturing the rhythmic nature of seizure activity [19], [20], [21]. A promising approach that balances computational cost and accuracy involves extracting time-domain features from specific frequency bands of interest in the EEG signal [15], [25]. This method allows for a focused analysis of the most relevant spectral components of the seizure activity while retaining the temporal dynamics of the signal.

However, the complex nature of EEG signals during seizures suggests that a more comprehensive approach to feature extraction might be beneficial. Model-based features, which attempt to capture the underlying stochastic properties of the EEG, have shown promise in this regard. Our previous work introduced an SMM for EEG analysis, which aims to capture both the non-Gaussian characteristics and amplitude information of EEG signals during seizures in a unified framework [23].

2) CLASSIFICATION MODELS
The choice of classifier is crucial in modeling the relationship between extracted features and seizure activity. Classifiers for

seizure detection can be broadly categorized into static and dynamic approaches.

Static classifiers, such as Support Vector Machines (SVM) [16], [26] and Multilayer Perceptron (MLP) [26], [27], have been widely used due to their computational efficiency and good performance on a variety of features. These methods treat each time point or window independently, which can be effective for many types of features. However, they may not fully capture the temporal dynamics of EEG signals during seizures, which can be critical for accurate detection.

Dynamic classifiers, on the other hand, explicitly model the temporal dependencies in the EEG signal. Hidden Markov models [28], [29] and RNNs [12], [30] are examples of such approaches. These methods can capture the evolving patterns of seizure activity over time, potentially leading to improved detection accuracy. In particular, the recent advancements in deep learning have led to the widespread use of RNN variants, such as Long Short-Term Memory (LSTM) and gated recurrent unit (GRU), in epileptic seizure detection tasks.

One particular dynamic classifier that has shown promise in biomedical signal analysis is the Recurrent Log-linearized Gaussian Mixture Network (R-LLGMN) [31]. This classifier is a time-series discriminative model that extends the Gaussian mixture model and hidden Markov model to an RNN framework. Its simple structure and effectiveness in scenarios with limited training data make it an interesting candidate for seizure detection tasks.

3) PROPOSED APPROACH

Building upon these existing methods, our work aims to combine the strengths of model-based feature extraction and dynamic classification. We propose to use features derived from the stochastic model, the SMM, of EEG, which captures both non-Gaussian characteristics and amplitude information, as inputs to an R-LLGMN classifier. This approach seeks to leverage the comprehensive signal representation provided by the SMM features while exploiting the temporal modeling capabilities of the R-LLGMN.

By integrating these components, we aim to address some of the challenges in inter-patient seizure detection, particularly in capturing the complex, non-Gaussian nature of EEG signals during seizures and modeling their temporal evolution.

B. SCALE MIXTURE MODEL OF EEG

The Scale Mixture Model [23] (SMM) describes the stochastic relationship between the recorded EEG signal $\mathbf{x} \in \mathbb{R}^D$ (D is the number of electrodes) and its covariance matrix. Although there are several variations of the SMM formulation, we follow the form used in our previous study, which uses a latent weight variable $u \in \mathbb{R}^+$ [32], [33].

In the model, the conditional distribution of the EEG signal $\mathbf{x}$, given u, is expressed via the multivariate Gaussian distribution with a mean vector of zero and a covariance

matrix of $u\mathbf{\Psi}$ as follows:

$$
\begin{aligned}
p(\mathbf{x}|u) &= \mathcal{N}(\mathbf{x}|\mathbf{0}, u\mathbf{\Psi}) \\
&= \frac{1}{(2\pi)^{D/2}|u\mathbf{\Psi}|^{1/2}} \exp\left[-\frac{1}{2u}\Delta\right],
\end{aligned} \tag{1}
$$

where $\mathbf{\Psi} \in \mathbb{R}^{D \times D}$ is the scale matrix of the EEG, and the covariance matrix $u\mathbf{\Psi}$ is represented by weighting $\mathbf{\Psi}$ with u. Δ is the Mahalanobis distance, defined as:

$$
\Delta = \mathbf{x}^\top \mathbf{\Psi}^{-1} \mathbf{x}. \tag{2}
$$

For the distribution of the latent variable u, we set an inverse gamma distribution:

$$
\begin{aligned}
p(u) &= \mathrm{IG}(u|\nu/2, \nu/2) \\
&= \frac{1}{\Gamma(\frac{\nu}{2})} \left(\frac{\nu}{2}\right)^{\frac{\nu}{2}} u^{-\frac{\nu}{2}-1} \exp\left(-\frac{\nu}{2u}\right),
\end{aligned} \tag{3}
$$

where $\nu \in \mathbb{R}^+$ is the degrees of freedom parameter.

Considering the marginal distribution of $\mathbf{x}$, the latent variable u can be integrated out as follows:

$$
\begin{aligned}
p(\mathbf{x}) &= \int p(\mathbf{x}|u)p(u)\mathrm{d}u \\
&= \int \mathcal{N}(\mathbf{x}|\mathbf{0}, u\mathbf{\Psi})\mathrm{IG}(u|\nu/2, \nu/2)\mathrm{d}u \\
&= \frac{\Gamma\left(\frac{\nu+D}{2}\right)}{\Gamma\left(\frac{\nu}{2}\right)} \frac{|\mathbf{\Psi}|^{-\frac{1}{2}}}{(\pi\nu)^{\frac{D}{2}}} \left[1 + \frac{\Delta}{\nu}\right]^{-\frac{\nu+D}{2}}.
\end{aligned} \tag{4} \tag{5}
$$

From (4), the EEG signal distribution $p(\mathbf{x})$ is modeled by summing an infinite number of Gaussian distributions with different covariance matrices, which enables the consideration of the amplitude uncertainty of EEG signals. In this representation, the SMM is parameterized by ν and $\mathbf{\Psi}$.

While previous work has demonstrated the effectiveness of SMM-derived features in distinguishing between seizure and non-seizure EEG segments [23], their potential in a practical seizure detection framework, particularly when combined with advanced classification techniques, remains to be fully explored. In this paper, we address this gap by integrating SMM-derived features with an RNN classifier.

III. METHODS

Fig. 1 shows an overview of the proposed epileptic seizure detection method. The proposed method consists of signal preprocessing, feature extraction based on the stochastic EEG model, and an epileptic seizure classifier. First, preprocessing removes muscle artifacts superimposed on EEG and extracts the bands that contain epileptic seizure features in the EEG signals. Second, the feature extraction provides non-Gaussianity and amplitude information of EEG signals based on the SMM. Finally, the epileptic seizure classifier uses a recurrent neural network, R-LLGMN, to calculate the posterior probability of the occurrence of an epileptic seizure by using features extracted from the EEG signals and to detect epileptic seizures.
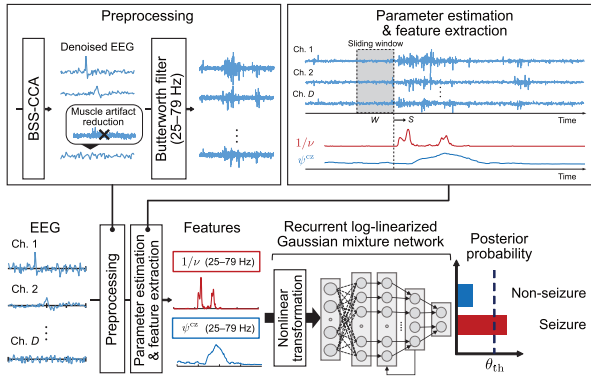
FIGURE 1. Overview of the proposed method. In the preprocessing stage, the γ band signal (25–79 Hz) is extracted using a bandpass filter after applying blind source separation based on canonical correlation analysis (BSS-CCA) for artifact removal from the measured EEG. Next, parameter estimation and feature extraction based on the stochastic EEG model are performed. The extracted features are then input into a recurrent log-linearized gaussian mixture network (R-LLGMN), which calculates the posterior probability for seizure/non-seizure by considering the temporal evolution of these features.

A. PREPROCESSING

Preprocessing aims to reduce artifacts in EEG signals and extract frequency band components that enable effective epileptic seizure detection. We apply a Blind Source Separation based on Canonical Correlation Analysis (BSS-CCA) [34], [35] to the EEG to reduce muscle artifacts in the signals. Let $\mathbf{X}^{\text{raw}} = \{\mathbf{x}_t^{\text{raw}} \in \mathbb{R}^D\}_{t=1}^T$ be the T points of raw EEG signals, where D is the number of channels. We assume that the EEG signals are obtained from a mixture of unknown signal sources $\mathbf{s}_t \in \mathbb{R}^D$. BSS aims to decompose the signal sources $\mathbf{s}_t$ from the observed signals by introducing a de-mixing matrix $\mathbf{W} \in \mathbb{R}^{D \times D}$ as follows:

$$\mathbf{s}_t = \mathbf{W}\mathbf{x}_t^{\text{raw}}. \tag{6}$$

In the BSS-CCA method, CCA is used to estimate signal sources. Let $\mathbf{y}_t^{\text{raw}} = \mathbf{x}_{t-1}^{\text{raw}}$ be the temporally delayed signals of the original EEG. We perform CCA for $\mathbf{x}_t^{\text{raw}}$ and $\mathbf{y}_t^{\text{raw}}$. Consequently, components are extracted such that the correlation coefficient between the EEG signal and its delayed version is maximized and regarded as the signal sources. Therefore, the obtained D signal sources are uncorrelated with each other, have maximum autocorrelation, and are ordered by decreasing autocorrelation index.

Muscle artifacts tend to have properties of temporal white noise rather than brain activity and, thus, present a low autocorrelation. Therefore, we set the columns that represent the activations of the components with low autocorrelation to zero in the mixing matrix $\mathbf{A} = \mathbf{W}^{-1}$ and reconstruct EEG from the sources.

$$\mathbf{x}_t^{\text{clean}} = \mathbf{A}^{\text{clean}}\mathbf{s}_t, \tag{7}$$

where $\mathbf{A}^{\text{clean}}$ is a mixing matrix in which the columns corresponding to muscle artifacts are set to zero. The above procedure reduces the influence of muscle artifacts in EEG.

Removing the muscle artifact component may cause the covariance matrix of $\mathbf{X}_t^{\text{clean}}$ to not be full rank. Hence,
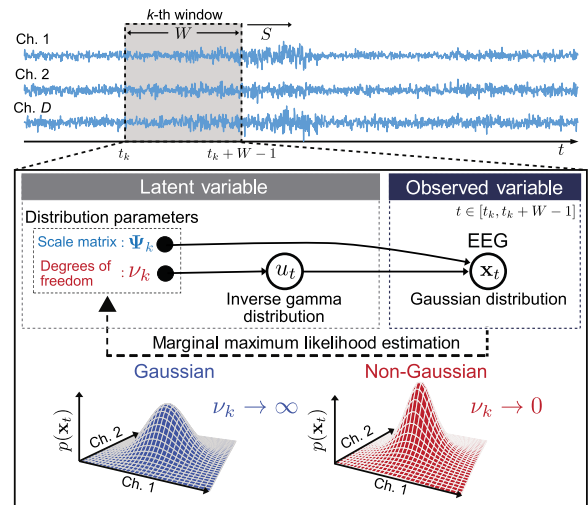

FIGURE 2. Graphical representation of the scale mixture model (SMM), which describes the stochastic relationship between an EEG signal $\{\mathbf{x}_t\}$ and its covariance matrix. The covariance matrix $u_t \Psi_k$ is determined by the random latent variable u_t and the scale matrix Ψ_k. The white nodes are random variables, and the black nodes are parameters to be estimated.

the parameter estimation of the stochastic model becomes inaccurate. We prevent the rank deficiency of the covariance matrix by adding a small amount of white noise, which follows a Gaussian distribution, $\mathcal{N}(0, s_d)$, to each dimension of $\mathbf{X}_t^{\text{clean}}$ independently. Here, s_d controls the noise amplitude and is set to $s_d = \varepsilon \sigma_d$, where σ_d is the standard deviation of the EEG signals in channel d and $\varepsilon \ll 1$ is a sufficiently small constant.

We then extract the components in a specific frequency band from EEG signals by using a third-order Butterworth band-pass filter. The filter passband was set to the γ band (25–79 Hz), a high-frequency band that well-reflects epileptic seizures, based on previous findings [23], [25], [36], [37]. Using this frequency band also has the advantage that low-frequency noise caused by cable oscillations can be ignored. The applied preprocessing allows for both the reduction of the influence of artifacts and extraction of representative EEG signals in a frequency band that suitably reflects epileptic seizure characteristics.

B. FEATURE EXTRACTION WITH SLIDING WINDOW

In this subsection, we describe the feature extraction of EEG signals using the SMM. For the preprocessed γ band signal $\mathbf{X} = \{\mathbf{x}_t\}_{t=1}^T$, we apply a moving window of length W and a slide width S. The signals within the k-th window are denoted as $\mathbf{X}_k = \{\mathbf{x}_t \mid t \in [t_k, t_k + W - 1]\}$, where $t_k = (k - 1)S + 1$ represents the start time of the k-th window. Here, the window index k ranges from 1 to K, where $K = \lfloor (T - W)/S \rfloor + 1$ is the total number of windows. We estimate the parameters of the SMM for the signals within each window and extract features from the estimated parameters (see Fig. 2).

1) PARAMETER ESTIMATION OF THE SCALE MIXTURE MODEL

Let us consider the estimation of the parameters of the SMM, ν_k and $\boldsymbol{\Psi}_k$, given the k-th window signals $\mathbf{X}_k$. The model parameters can be estimated by maximizing the marginal likelihood

$$p(\mathbf{X}_k) = \prod_{t=t_k}^{t_k+W-1} p(\mathbf{x}_t). \tag{8}$$

We conduct this optimization for ν_k and $\boldsymbol{\Psi}_k$ based on the Expectation-Maximization (EM) algorithm [38]. The EM algorithm iterates via the application of an expectation step (E-step) and a maximization step (M-step).

The estimation procedures are as follows:

 (i) Initialize each parameter by selecting arbitrary starting values.

 (ii) *E-step*. Calculate the expectation of the complete-data log-likelihood, denoted as $Q(\nu_k, \boldsymbol{\Psi}_k)$.

$$
\begin{aligned}
& Q(\nu_k, \boldsymbol{\Psi}_k) \\
&= \mathbb{E}\left[\ln \prod_{t=t_k}^{t_k+W-1} \mathrm{IG}(u_t \mid \nu_k/2, \nu_k/2)\mathcal{N}(\mathbf{x}_t|\mathbf{0}, u_t\boldsymbol{\Psi}_k)\right] \\
&= \sum_{t=t_k}^{t_k+W-1}\left[-\frac{D}{2}\ln(2\pi) - \frac{D}{2}\mathbb{E}\left[\ln u_t\right] - \frac{1}{2}\ln|\boldsymbol{\Psi}_k|\right. \\
&\quad - \frac{1}{2}\mathbb{E}\left[u_t^{-1}\right]\Delta_t + \frac{\nu_k}{2}\ln\frac{\nu_k}{2} - \ln\Gamma\left(\frac{\nu_k}{2}\right) \\
&\quad \left. - \left(\frac{\nu_k}{2}+1\right)\mathbb{E}\left[\ln u_t\right] - \frac{\nu_k}{2}\mathbb{E}\left[u_t^{-1}\right]\right],
\end{aligned} \tag{9}
$$

where $\mathbb{E}\left[u_t^{-1}\right]$ and $\mathbb{E}\left[\ln u_t\right]$ are derived by calculating the posterior distribution $p(u_t|\mathbf{x}_t)$ of the latent variable u_t as follows:

$$\mathbb{E}\left[u_t^{-1}\right] = \frac{\nu_k + D}{\nu_k + \Delta_t}, \tag{10}$$

$$\mathbb{E}\left[\ln u_t\right] = -\ln\mathbb{E}\left[u_t^{-1}\right] + \ln\left(\frac{\nu_k+D}{2}\right) - \phi\left(\frac{\nu_k+D}{2}\right), \tag{11}$$

where $\phi(\cdot)$ is the digamma function.

 (iii) *M-step*. Update the parameters by maximizing $Q(\nu_k, \boldsymbol{\Psi}_k)$. By setting the derivative of $Q(\nu_k, \boldsymbol{\Psi}_k)$ with respect to $\boldsymbol{\Psi}_k$ equal to zero, the new scale matrix is obtained as

$$^{\text{new}}\boldsymbol{\Psi}_k = \frac{1}{t_k+W-1}\sum_{t=t_k}^{t_k+W-1}\mathbb{E}\left[u_t^{-1}\right]\mathbf{x}_t\mathbf{x}_t^{\top}. \tag{12}$$

Because a closed-form expression for the degrees of freedom parameter ν_k does not exist, we estimate ν_k by iteratively maximizing $Q(\nu_k, \boldsymbol{\Psi}_k)$ using the bisection method.

$$^{\text{new}}\nu_k = \arg\max_{\nu_k} Q(\nu_k, {}^{\text{new}}\boldsymbol{\Psi}_k). \tag{13}$$

Algorithm 1 Proposed EEG Feature Extraction Procedure

Input: Raw EEG signal $\mathbf{X}^{\text{raw}} = \{\mathbf{x}_t^{\text{raw}}\}_{t=1}^T$, window length W, window stride S
Output: Feature vector $\{\mathbf{z}_k\}_{k=1}^K$
$\mathbf{X}^{\text{clean}} = \text{BSS-CCA}(\mathbf{X}^{\text{raw}})$;   // Clean signals
$\mathbf{X} = \text{Bandpass}(\mathbf{X}^{\text{clean}})$;   // Extract γ band
$K = \lfloor(T-W)/S\rfloor + 1$
for $k \leftarrow 1$ **to** K **do**
   $t_k = (k-1)S + 1$;
   $\mathbf{X}_k = \{\mathbf{x}_t \mid t \in [t_k, t_k + W - 1]\}$;
   $\mathbf{z}_k = \text{ComputeFeature}(\mathbf{X}_k)$;

return $\{\mathbf{z}_k\}_{k=1}^K$;
Function *ComputeFeature*$(\mathbf{X}_k)$**:**
   Initialize ν_k and $\boldsymbol{\Psi}_k$;
   while $\ln p(\mathbf{X}_k)$ *have not converged* **do**
      Calculate $\mathbb{E}[u_t^{-1}]$ and $\mathbb{E}[\ln u_t]$ using (10) and (11) ;
      Update ν_k and $\boldsymbol{\Psi}_k$ using (13) and (12);
   return $\mathbf{z}_k = [1/\nu_k, \psi_k^{\text{cz}}]^{\top}$;

 (iv) Evaluate the log-likelihood $\ln p(\mathbf{X}_k)$ and repeat steps (ii)–(iv) until the calculation converges.

This optimization step promotes convergence towards a local optimum by exploiting the monotonic increase in likelihood guaranteed by the EM algorithm [39]. While the computational cost depends on the input dimensionality and window length, convergence is achieved in approximately 0.2 s under our experimental conditions. We have examined the computational cost in detail in our previous work [23].

In the SMM framework, the non-Gaussianity of EEG signals is modeled through the stochastic fluctuation of the covariance matrix, which is controlled by the latent variable u_t. This statistical representation corresponds to subtle variations in the EEG amplitude in the observed data. Therefore, by estimating ν_k and $\boldsymbol{\Psi}_k$ from the EEG signals, the stochastic fluctuation and magnitude of the EEG amplitude can be evaluated.

2) FEATURE EXTRACTION

We extract temporal features to detect epileptic seizures based on the estimated model parameters, ν_k and $\boldsymbol{\Psi}_k$, for the k-th window. Here, we focus on the non-Gaussianity of EEG signals and amplitude information that are generally considered effective for epileptic seizure detection [9].

Based on our previous study [23], we calculate $1/\nu_k$, the reciprocal of ν_k, as a non-Gaussianity feature characterizing a stochastic fluctuation in EEG amplitude. In the preliminary evaluation, the network training became very unstable when all dimensions of $\boldsymbol{\Psi}_k$ were used as inputs. Therefore, a single element ψ_k^{cz} corresponding to the electrode Cz is extracted from $\boldsymbol{\Psi}_k$ and used as a feature value. The Cz channel is located at the center of the scalp and is expected to be able
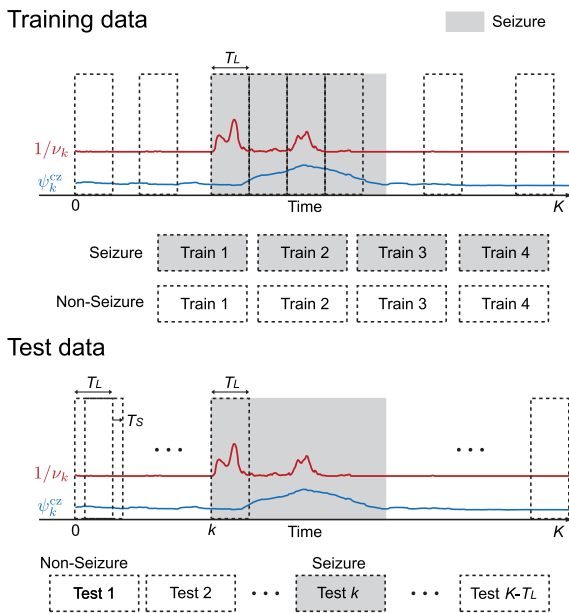
FIGURE 3. Splitting of the training and test data for R-LLGMN. For the training data, features of length T_L are extracted from the beginning of the seizure segment without overlapping, and are used as the training data for the seizure class. An equal number of features are randomly extracted from the non-seizure segment and used as the training data for the non-seizure class. For the test data, features are extracted in a sliding window of length T_L, and the test data are obtained by moving the sliding window by T_S.

to detect seizures occurring in both hemispheres in a stable manner [40], [41].

Based on the above, we extract the feature vector $\mathbf{z}_k = [1/\nu_k, \psi_k^{\mathrm{cz}}]^\top$ for each window. Algorithm 1 shows the procedure for extracting the feature vector. By using the time series of this feature vector $\{\mathbf{z}_k\}_{k=1}^K$ as input to the classifier, we can detect seizures by considering the stochastic fluctuation (i.e., non-Gaussianity) and magnitude of EEG amplitude. Hereafter, we omit the subscript k for the window index when it is not necessary.

C. AUTOMATIC SEIZURE DETECTION

We segment the extracted features $\{\mathbf{z}_k\}_{k=1}^K$ for both training and testing purposes, as illustrated in Fig. 3 for seizure detection. To address the common imbalance between seizure and non-seizure data points, we balance the training data by extracting an equal number of points for each class. For the seizure class, we extract features from the beginning of seizure segments for a time length T_L without overlapping. For the non-seizure class, we randomly extract the same number of features, also of length T_L, from non-seizure segments. For testing, we apply a sliding window of length T_L to the calculated features, moving it by T_S over the test data. After segmentation, we normalize both training and test data according to the mean and standard deviation of the training data.

An RNN is used as a detection model for seizure detection, taking into account temporal changes in the extracted features. As a specific architecture, we use the R-LLGMN [31], which has a simple structure but shows excellent performance
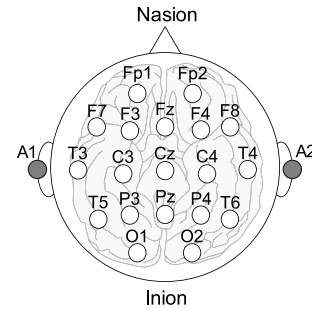

FIGURE 4. International 10–20 electrode montage. The 19-channel surface electrodes are placed on the scalp according to the international 10–20 electrode placement system, with reference electrodes on both earlobes: A1 and A2.

in biological signal recognition. The R-LLGMN incorporates a hidden Markov model with Gaussian mixture models as the output probability distributions in its network structure, enabling pattern classification that considers the time-series characteristics of the input data. The R-LLGMN allows for seizure detection, considering the temporal variation of feature vectors within a time length of T_L.

The R-LLGMN is trained by minimizing the cross-entropy loss for seizure and non-seizure training data based on the backpropagation through time method [42]. The test data are then input into the trained R-LLGMN, and the posterior probabilities for each class are calculated. If the posterior probability of the seizure class exceeds a threshold value θ_{th}, then the corresponding data are determined to represent a seizure; otherwise, they are classified as non-seizure.

IV. EXPERIMENTS

A. DATASET

To verify the classification performance of the proposed method, we conducted an experiment to detect epileptic seizures. In this experiment, we used a dataset of 20 patients with focal epilepsy presented in [23]. The patients' information is summarized in Table 1. Each patient had one seizure recording. The EEG signals were recorded at a digital sampling frequency of $f_s = 500$ Hz using an EEG system (Neurofax EEG-1218, Nihon Kohden, Tokyo, Japan), while the patients were lying in the supine position. Nineteen-channel surface electrodes ($D = 19$) were placed on the scalp of each patient according to the international 10–20 electrode placement system, with reference electrodes on both earlobes: A1 and A2 (see Fig. 4).

The onset and offset of a focal seizure in each EEG recording were marked by a board-certified epileptologist (T.A.). Written informed consent was obtained from all patients. The experiments were approved by the Okayama University Ethics Committee (approval No: 1706–019). For the analysis, each EEG recording was clipped to approximately 240–420 s, including the pre- and post-seizure segments.

B. EXPERIMENTAL CONDITIONS

During EEG signal preprocessing, components with an autocorrelation coefficient of CCA $\rho < 0.99$ were removed

TABLE 1. Patient conditions.

Patient	Sex	Age (year)	Total data length (s)	Seizure duration (s)
A	Male	2	300	71
B	Male	23	300	54
C	Female	4	300	31
D	Male	4	380	93
E	Male	0.5	320	39
F	Male	41	300	32
G	Female	3	240	53
H	Male	19	390	36
I	Male	0.8	390	98
J	Male	20	360	16
K	Male	36	300	23
L	Male	9	300	43
M	Male	13	300	43
N	Male	15	300	48
O	Male	8	300	17
P	Female	19	300	69
Q	Male	27	420	62
R	Male	38	300	65
S	Male	17	300	17
T	Male	19	300	65

FIGURE 5. Averaged performance metrics for the proposed method according to time length $T'_L = T_L/f_s$ over patients. The results were calculated based on the leave-one-patient-out cross-validation.

as muscle artifacts. For feature extraction of $1/\nu_k$ and ψ_k^{cz}, the length of the sliding window W and slide width S were set to 7,500 (i.e., 15 s) and 500 (i.e., 1 s), respectively; these settings were the same as those used by Furui et al. [23]. With this setup, the features were calculated every second. We searched for the optimal value of time length T_L when selecting data segments for epileptic seizure classification. In the dataset, the shortest epileptic seizure duration was 16 s; therefore, we evaluated the classification performance by setting the time length to $T_L = 500, 1500, 2500, \ldots, 7500$. Given the sampling frequency $f_s = 500$ Hz, this corresponds to a time window of $T'_L = T_L/f_s = 1, 3, 5, \ldots, 15$ s. We set $T_S = S$.

To evaluate the classification performance, leave-one-patient-out cross-validation was applied to the dataset. This validation used data extracted from 19 patients for training and data from the remaining patient for testing. For the 20 cross-validation experiments, we calculated the mean and standard error of the following evaluation metrics: accuracy, precision, sensitivity, specificity, Matthews Correlation Coefficient (MCC), the Area Under the Receiver Operating Characteristic Curve (AUC-ROC), and the Area Under the Precision-Recall Curve (AUC-PR). This multi-metric approach provides a balanced perspective, particularly in detecting infrequent yet critically important seizure events. It allows us to capture aspects of performance that might be obscured by accuracy metrics alone in imbalanced datasets.

The training of the R-LLGMN employed stochastic gradient descent with a batch size of 32 and a learning rate of 0.001. The number of epochs was set to 100. The hyperparameters of the R-LLGMN were set to state $K = 2$ and component $M_c = 1$. The threshold of the posterior probability, θ_{th}, was set to the value that gave the maximum F1 score on the precision-recall curve. This threshold calculation was performed for the training data, and the same value was applied to the test data.
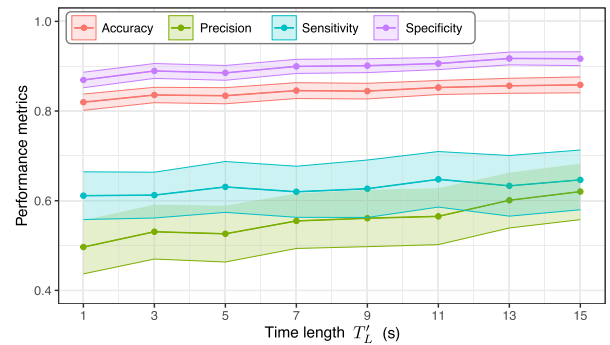
C. ABLATION STUDY

We conducted two ablation studies to investigate the effectiveness of the proposed method over existing methodologies. In this evaluation, we fixed the time length to $T'_L = T_L/f_s = 15$ s.

First, we evaluated the performance when the classification model in the proposed method was replaced with other models. We used three static models—MLP, SVM, and Log-linearized Gaussian Mixture Network (LLGMN) [43]—and one dynamic model, LSTM, as comparison models. The MLP had one hidden layer with 64 units and used the ReLU activation function. The SVM used the radial basis function kernel with the kernel coefficient set to 0.5. The LLGMN was equivalent to the R-LLGMN with the dynamic structure removed (i.e., $T_L = 1, K = 1, M_c = 1$).

Next, we compared the performance when the input features of the proposed method were replaced. As existing features, we used the variance (Var) [17], the third-order cumulant (ToC) [18], and the approximate entropy (ApEn) [15] of the EEG signals. Additionally, we evaluated the performance when the proposed feature set was combined with these existing features.

D. PATIENT-SPECIFIC ANALYSIS

We performed a patient-specific analysis to evaluate the sensitivity and specificity of the proposed method. We compared the performance of the proposed method with that of Persyst P13 (Persyst Development, San Diego, CA, USA), a commercially available EEG classification program with automatic seizure detection. For Persyst, the raw recorded EEG signals were used as an input, and its seizure detection outputs were evaluated. It should be noted that Persyst was not trained using our dataset because it uses a built-in pre-trained model.

V. RESULTS

Fig. 5 shows the averaged accuracy, precision, sensitivity, and specificity obtained from the proposed method according to time length $T'_L = T_L/f_s$. All metrics increased as T'_L increased, and the highest values were obtained when $T'_L = 15$ s. Fig. 6 shows examples of seizure detection results for Patients C, M, and Q. In the figure, the raw EEG
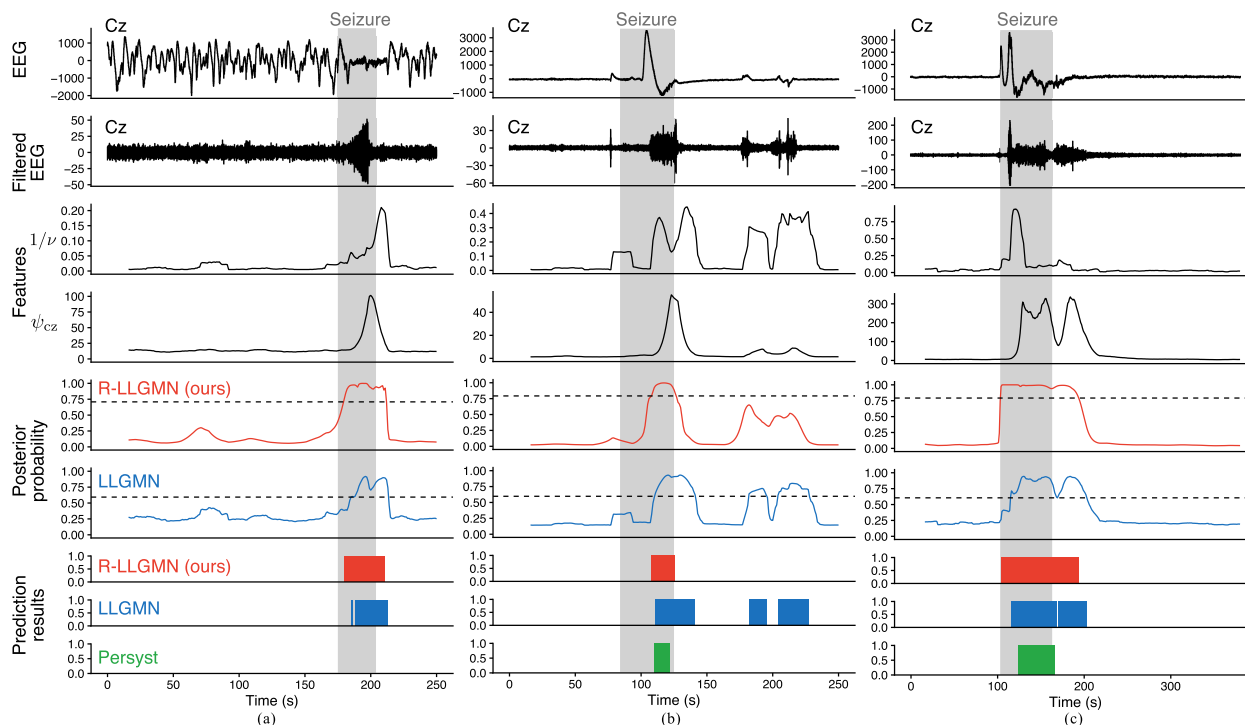
FIGURE 6. Examples of seizure detection results for (a) Patient C, (b) Patient M, and (c) Patient Q. The shaded area represents the epileptic seizure occurrence annotated by an epileptologist. The dashed lines in the posterior probability plots are the seizure detection thresholds, which are adjusted for each validation fold.

TABLE 2. Performance metrics for each classification model (*mean ± standard deviation*). Best performance is indicated in bold while the second best is underlined.

Model	Accuracy	Precision	Sensitivity	Specificity	MCC	AUC-ROC	AUC-PR
MLP	0.831 ± 0.082	0.521 ± 0.258	0.593 ± 0.223	0.886 ± 0.075	0.438 ± 0.225	$\underline{0.860 \pm 0.097}$	0.553 ± 0.263
SVM	0.829 ± 0.081	0.515 ± 0.264	0.562 ± 0.213	0.887 ± 0.071	0.420 ± 0.233	0.707 ± 0.124	0.478 ± 0.210
LLGMN	0.826 ± 0.081	0.504 ± 0.264	$\mathbf{0.649 \pm 0.193}$	0.867 ± 0.079	0.457 ± 0.232	0.857 ± 0.098	0.541 ± 0.263
LSTM	$\underline{0.843 \pm 0.085}$	$\underline{0.588 \pm 0.283}$	0.631 ± 0.314	$\underline{0.898 \pm 0.073}$	$\underline{0.497 \pm 0.276}$	$\mathbf{0.875 \pm 0.144}$	$\mathbf{0.688 \pm 0.271}$
R-LLGMN (**ours**)	$\mathbf{0.858 \pm 0.079}$	$\mathbf{0.620 \pm 0.280}$	$\underline{0.647 \pm 0.298}$	$\mathbf{0.917 \pm 0.069}$	$\mathbf{0.529 \pm 0.258}$	0.852 ± 0.168	$\underline{0.661 \pm 0.287}$

waveforms, preprocessed waveforms, features $1/\nu$ and ψ^{cz}, posterior probabilities, and their seizure detection results are illustrated in order, from the top. The prediction results are shown for the proposed method using R-LLGMN, its static version LLGMN, and the commercially available software Persyst. The gray-shaded areas indicate the epileptic seizure occurrences as diagnosed by an epileptologist. The EEG waveforms are shown only for the Cz channel.

The results of the ablation study are shown in Table 2 for the classification models and in Table 3 for the input features. Table 2 lists the performance metrics for each classification model. Overall, the dynamic classifiers (i.e., LSTM and R-LLGMN) tended to show better performance. In particular, the proposed method with R-LLGMN outperformed the comparison models in terms of accuracy, precision, specificity, and MCC. Table 3 lists the performance metrics for each input feature. The proposed feature set alone or in combination with existing features tended to outperform the existing features. Specifically, the proposed feature set alone showed better performance in terms of precision and MCC, while the combination of the proposed feature set and ApEn

showed better performance in terms of accuracy, specificity, and AUC.

Table 4 summarizes the patient-specific sensitivity and specificity. We performed the McNemar test (significance level: 5%) for the sensitivity and specificity of each patient to compare these metrics between the proposed method and Persyst. For sensitivity, significantly higher proportions ($p < 0.05$) occurred in 10 patients for the proposed method and in five patients for Persyst. For specificity, significantly higher proportions occurred in one patient for the proposed method and in 13 patients for Persyst. Additionally, the proposed method exhibited non-zero sensitivity for all patients, which means that the proposed method detected epileptic seizures in every patient correctly.

VI. DISCUSSION
In this paper, we proposed an epileptic seizure detection method that utilizes a stochastic EEG model with a scale mixture structure. In the proposed method, two features, namely, the non-Gaussianity and amplitude information of EEG, are calculated based on the stochastic model. The seizure

TABLE 3. Performance metrics for each feature set (*mean ± standard deviation*). The '+' symbol denotes the combination of each feature along the input dimension. Best performance is indicated in bold while the second best is underlined.

Feature set	Accuracy	Precision	Sensitivity	Specificity	MCC	AUC-ROC	AUC-PR
Var	0.852 ± 0.075	0.563 ± 0.312	0.661 ± 0.286	0.900 ± 0.068	0.508 ± 0.285	$\mathbf{0.875 \pm 0.116}$	0.598 ± 0.307
ToC	0.797 ± 0.120	0.462 ± 0.332	$\mathbf{0.695 \pm 0.355}$	0.825 ± 0.129	0.431 ± 0.350	0.854 ± 0.150	0.647 ± 0.290
ApEn	0.459 ± 0.175	0.201 ± 0.123	0.613 ± 0.246	0.421 ± 0.245	0.024 ± 0.198	0.561 ± 0.215	0.350 ± 0.288
Var + ToC + ApEn	0.846 ± 0.069	0.520 ± 0.355	0.534 ± 0.307	0.907 ± 0.072	0.426 ± 0.323	0.786 ± 0.207	0.555 ± 0.336
$1/\nu + \psi^{\mathrm{cz}}$ (**ours**)	$\underline{0.858 \pm 0.079}$	$\mathbf{0.620 \pm 0.280}$	0.647 ± 0.298	0.917 ± 0.069	$\mathbf{0.529 \pm 0.258}$	0.852 ± 0.168	$\underline{0.661 \pm 0.287}$
+ Var	0.849 ± 0.082	0.560 ± 0.337	0.570 ± 0.299	$\underline{0.918 \pm 0.072}$	0.466 ± 0.309	0.822 ± 0.192	0.593 ± 0.305
+ ToC	0.849 ± 0.068	0.554 ± 0.327	0.593 ± 0.282	0.912 ± 0.076	0.475 ± 0.273	0.801 ± 0.214	0.550 ± 0.289
+ ApEn	$\mathbf{0.861 \pm 0.062}$	$\underline{0.608 \pm 0.289}$	0.598 ± 0.274	$\mathbf{0.925 \pm 0.056}$	$\underline{0.508 \pm 0.242}$	$\underline{0.861 \pm 0.150}$	$\mathbf{0.662 \pm 0.271}$
+ Var + ToC + ApEn	0.855 ± 0.080	0.551 ± 0.332	0.598 ± 0.310	0.912 ± 0.070	0.478 ± 0.315	0.826 ± 0.167	0.611 ± 0.277

TABLE 4. Sensitivity and specificity for each patient. Superior performance is indicated in bold.

Patient	Sensitivity		Specificity	
	Ours	Persyst	Ours	Persyst
A	**0.971****	0.000	0.911	**0.994****
B	**0.792****	0.000	0.970	0.995
C	**0.833****	0.000	0.968	0.995*
D	0.663	**0.815***	0.928	**1.000****
E	**0.026**	0.000	0.927	**0.996***
F	**0.625****	0.000	0.826	**0.995****
G	**0.528****	0.000	0.957	**0.993**
H	**0.857***	0.657	0.935	**0.987****
I	0.897	**1.000****	**1.000****	0.938
J	**1.000****	0.000	0.852	**0.916***
K	**0.954**	0.773	0.895	**0.996****
L	0.405	**0.857****	**0.957**	0.933
M	**0.429**	0.310	**0.995**	**0.995**
N	0.500	**0.604**	0.739	**0.926****
O	**0.500****	0.000	0.791	**0.996****
P	0.500	**0.794****	0.896	**0.983****
Q	**0.984****	0.656	0.904	**0.994****
R	**0.385****	0.000	0.941	**0.995****
S	**1.000**	0.882	0.940	**0.949**
T	0.080	**1.000****	**1.000**	0.972
Average	**0.647**	0.417	0.917	**0.977**

*, ** : significantly higher proportions with the proposed method and Persyst as indicated by the patient-wise McNemar test (*: $p < 0.05$, **: $p < 0.01$).

probability is then calculated by inputting the time-series changes of the features into a recurrent neural network. In the experiment, we investigated the performance of seizure detection on a dataset of 20 epilepsy patients. To evaluate the effectiveness of the proposed method, we conducted a comprehensive assessment encompassing several aspects: performance evaluation across varying time lengths for segmentation, efficacy of the dynamic structure, effectiveness of the feature set, and patient-specific performance analysis.

All the evaluation metrics increased as time length $T'_L = T_L/f_s$ increased (Fig. 5). Therefore, the proposed method with a long observation time can properly learn the temporal changes in the features of epileptic seizures, which typically last for on the order of tens of seconds. However, for real-time seizure detection, a longer T'_L setting requires more data buffer capacity, resulting in an increased time delay in detection. Depending on the degree of immediacy required for the detection, the time length setting may require adjustment.

Dynamic classifiers demonstrated superior performance compared to static classifiers (Table 2). This result can be attributed to the ability of time-varying structures to adequately capture the non-stationarity of EEG signals. Furthermore, observation of the differences in posterior probabilities between R-LLGMN and its static counterpart, LLGMN (Fig. 6), suggests that classifiers with dynamic structures can mitigate abrupt changes in posterior probabilities, thereby reducing false positives. Among the dynamic classifiers, R-LLGMN slightly outperformed LSTM, likely due to its simpler structure. While R-LLGMN may not be capable of learning long-term and complex dependencies like LSTM, it appears to possess sufficient learning capacity for problems involving relatively short-term temporal changes, such as the one addressed in this study. These findings demonstrate that considering the temporal evolution of the proposed feature set, including non-Gaussianity and amplitude, enables appropriate detection of epileptic seizures.

The proposed feature set demonstrated overall superior performance compared to existing feature sets (Table 3). Analysis of the examples in Fig. 6 reveals that $1/\nu$ tends to respond strongly to signal non-stationarity, capturing characteristics distinct from simple amplitude variations. This suggests that the combination of $1/\nu$ with ψ^{cz}, which reflects amplitude, effectively contributes to the comprehensive evaluation based on the stochastic model. Furthermore, integrating the proposed feature set with existing methods yielded overall performance improvements compared to the existing methods alone. Interestingly, combining the proposed features with ApEn [15], which individually showed notably low precision and specificity, resulted in the best specificity and AUC-PR scores. This improvement can be attributed to ApEn capturing signal pattern complexity from a different perspective than the proposed $1/\nu$ feature, enabling a more comprehensive evaluation when used in combination. In conclusion, the proposed feature set demonstrates its efficacy both independently and as a valuable complement to existing feature sets, offering a more comprehensive approach to signal analysis in this context.

The proposed method tends to provide a higher sensitivity than Persyst (Table 4). Moreover, as illustrated in Fig. 6, while

Persyst completely missed the detection for some patients, the proposed method successfully detected seizures across all patients. However, the specificity of Persyst tends to be higher than that of the proposed method. To reduce the false alarm rate in clinical settings, Persyst only indicates the occurrence of a seizure if the seizure probability exceeds a certain value for more than 11 s [44]. Therefore, while seizure detection tends to fail in patients with short seizure segments, false positives due to noise are suppressed in Persyst, resulting in higher specificity. This specificity satisfies clinical requirements to minimize false-positive rates as much as possible. However, for patients with frequent epileptic seizures, where detailed seizure detection is crucial, it is necessary to maximize sensitivity while maintaining a minimum level of specificity. In this regard, the proposed method demonstrates superiority by achieving excellent sensitivity with only a slight compromise in specificity.

VII. CONCLUSION

In this paper, we presented an automatic epileptic seizure detection method using a recurrent neural network with input features obtained from a scale mixture-based stochastic EEG model, the SMM. In the proposed method, after applying preprocessing to EEG signals, features reflecting the non-Gaussianity and amplitude of the signals are extracted based on the stochastic model. Subsequently, epileptic seizures can be detected using these features as the input to a classifier with a dynamic structure.

We experimentally evaluated the epileptic seizure classification performance using EEG recordings from 20 patients diagnosed with focal epilepsy. Our ablation study of classifiers and features demonstrated the effectiveness of each component in the proposed method. The class of dynamic classifiers, particularly the R-LLGMN adopted in our approach, exhibited superior performance in epileptic seizure detection. Furthermore, our proposed feature set demonstrated dual efficacy: it outperformed existing feature sets when used alone and enhanced performance when combined with them. These findings validate both the individual and combined strengths of our method's core elements. The demonstrated robustness of our proposed features in epileptic seizure detection tasks highlights the potential of our approach for advancing automated epileptic seizure detection.

In this study, seizure detection was conducted on patients with focal epilepsy. However, as the statistical characteristics of EEG signals differ depending on the type of seizure [45], a model created for one type may not be effective for other types. In future research, we will investigate the generalization performance of the proposed method by increasing the number of seizure types and extending analysis times. We also plan to extend the stochastic EEG model by including features related to skewness [46], which are independent of the features used in this study, to further improve epileptic seizure detection.

REFERENCES

[1] World Health Org. (2019). *Epilepsy Fact Sheet*. [Online]. Available: https://www.who.int/news-room/fact-sheets/detail/epilepsy

[2] E. R. Kandel, J. H. Schwartz, T. M. Jessell, M. B. T. Jessell, S. Siegelbaum, and A. Hudspeth, *Principles of Neural Science*. New York, NY, USA: McGraw-Hill, 2000.

[3] R. S. Fisher, W. V. E. Boas, W. Blume, C. Elger, P. Genton, P. Lee, and J. Engel, "Epileptic seizures and epilepsy: Definitions proposed by the international league against epilepsy (ILAE) and the international bureau for epilepsy (IBE)," *Epilepsia*, vol. 46, no. 4, pp. 470–472, Mar. 2005.

[4] A. H. Shoeb and J. V. Guttag, "Application of machine learning to epileptic seizure detection," in *Proc. 27th Int. Conf. Mach. Learn.*, 2010, pp. 975–982.

[5] P. Mirowski, D. Madhavan, Y. LeCun, and R. Kuzniecky, "Classification of patterns of EEG synchronization for seizure prediction," *Clin. Neurophysiol.*, vol. 120, no. 11, pp. 1927–1940, Nov. 2009.

[6] M. Zabihi, S. Kiranyaz, A. B. Rad, A. K. Katsaggelos, M. Gabbouj, and T. Ince, "Analysis of high-dimensional phase space via Poincaré section for patient-specific seizure detection," *IEEE Trans. Neural Syst. Rehabil. Eng.*, vol. 24, no. 3, pp. 386–398, Mar. 2016.

[7] A. Van Esbroeck, L. Smith, Z. Syed, S. Singh, and Z. Karam, "Multi-task seizure detection: Addressing intra-patient variation in seizure morphologies," *Mach. Learn.*, vol. 102, no. 3, pp. 309–321, Mar. 2016.

[8] C. Gómez, P. Arbeláez, M. Navarrete, C. Alvarado-Rojas, M. Le Van Quyen, and M. Valderrama, "Automatic seizure detection based on imaged-EEG signals through fully convolutional networks," *Sci. Rep.*, vol. 10, no. 1, p. 21833, Dec. 2020.

[9] B. R. Greene, S. Faul, W. P. Marnane, G. Lightbody, I. Korotchikova, and G. B. Boylan, "A comparison of quantitative EEG features for neonatal seizure detection," *Clin. Neurophysiol.*, vol. 119, no. 6, pp. 1248–1261, Jun. 2008.

[10] L. Orosco, A. G. Correa, P. Diez, and E. Laciar, "Patient non-specific algorithm for seizures detection in scalp EEG," *Comput. Biol. Med.*, vol. 71, pp. 128–134, Apr. 2016.

[11] M. Mohammadi, N. A. Khan, and A. A. Pouyan, "Automatic seizure detection using a highly adaptive directional time–frequency distribution," *Multidimensional Syst. Signal Process.*, vol. 29, no. 4, pp. 1661–1678, Oct. 2018.

[12] J. Craley, E. Johnson, C. Jouny, and A. Venkataraman, "Automated inter-patient seizure detection using multichannel convolutional and recurrent neural networks," *Biomed. Signal Process. Control*, vol. 64, Feb. 2021, Art. no. 102360.

[13] H. Khamis, A. Mohamed, and S. Simpson, "Seizure state detection of temporal lobe seizures by autoregressive spectral analysis of scalp EEG," *Clin. Neurophysiol.*, vol. 120, no. 8, pp. 1479–1488, Aug. 2009.

[14] G. R. Minasyan, J. B. Chatten, M. J. Chatten, and R. N. Harner, "Patient-specific early seizure detection from scalp EEG," *J. Clin. Neurophysiol.*, vol. 27, no. 3, pp. 163–178, Jun. 2010.

[15] V. Srinivasan, C. Eswaran, and N. Sriraam, "Approximate entropy-based epileptic EEG detection using artificial neural networks," *IEEE Trans. Inf. Technol. Biomed.*, vol. 11, no. 3, pp. 288–295, May 2007.

[16] R. Sharma, R. B. Pachori, and P. Sircar, "Seizures classification based on higher order statistics and deep neural network," *Biomed. Signal Process. Control*, vol. 59, May 2020, Art. no. 101921.

[17] S. Yang, B. Li, Y. Zhang, M. Duan, S. Liu, Y. Zhang, X. Feng, R. Tan, L. Huang, and F. Zhou, "Selection of features for patient-independent detection of seizure events using scalp EEG signals," *Comput. Biol. Med.*, vol. 119, Apr. 2020, Art. no. 103671.

[18] R. Sharma, P. Sircar, and R. B. Pachori, "Automated focal EEG signal detection based on third order cumulant function," *Biomed. Signal Process. Control*, vol. 58, Apr. 2020, Art. no. 101856.

[19] A. T. Tzallas, M. G. Tsipouras, and D. I. Fotiadis, "Epileptic seizure detection in EEGs using time–frequency analysis," *IEEE Trans. Inf. Technol. Biomed.*, vol. 13, no. 5, pp. 703–710, Sep. 2009.

[20] H. Chu, C. K. Chung, W. Jeong, and K.-H. Cho, "Predicting epileptic seizures from scalp EEG based on attractor state analysis," *Comput. Methods Programs Biomed.*, vol. 143, pp. 75–87, May 2017.

[21] D. Wang, D. Ren, K. Li, Y. Feng, D. Ma, X. Yan, and G. Wang, "Epileptic seizure detection in long-term EEG recordings by using wavelet-based directed transfer function," *IEEE Trans. Biomed. Eng.*, vol. 65, no. 11, pp. 2591–2599, Nov. 2018.

[22] M. Nurujjaman, R. Narayanan, and A. S. Iyengar, "Comparative study of nonlinear properties of EEG signals of normal persons and epileptic patients," *Nonlinear Biomed. Phys.*, vol. 3, no. 1, p. 6, Dec. 2009.

[23] A. Furui, R. Onishi, A. Takeuchi, T. Akiyama, and T. Tsuji, "Non-Gaussianity detection of EEG signals based on a multivariate scale mixture model for diagnosis of epileptic seizures," *IEEE Trans. Biomed. Eng.*, vol. 68, no. 2, pp. 515–525, Feb. 2021.

[24] M. Tajmirriahi and Z. Amini, "Modeling of seizure and seizure-free EEG signals based on stochastic differential equations," *Chaos, Solitons Fractals*, vol. 150, Sep. 2021, Art. no. 111104.

[25] M. Sameer, A. K. Gupta, C. Chakraborty, and B. Gupta, "Epileptical seizure detection: Performance analysis of gamma band in EEG signal using short-time Fourier transform," in *Proc. 22nd Int. Symp. Wireless Pers. Multimedia Commun. (WPMC)*, Nov. 2019, pp. 1–6.

[26] E. Alickovic, J. Kevric, and A. Subasi, "Performance evaluation of empirical mode decomposition, discrete wavelet transform, and wavelet packed decomposition for automated epileptic seizure detection and prediction," *Biomed. Signal Process. Control*, vol. 39, pp. 94–102, Jan. 2018.

[27] S. M. Ghazali, M. Alizadeh, J. Mazloum, and Y. Baleghi, "Modified binary salp swarm algorithm in EEG signal classification for epilepsy seizure detection," *Biomed. Signal Process. Control*, vol. 78, Sep. 2022, Art. no. 103858.

[28] J. Craley, E. Johnson, and A. Venkataraman, "A spatio-temporal model of seizure propagation in focal epilepsy," *IEEE Trans. Med. Imag.*, vol. 39, no. 5, pp. 1404–1418, May 2020.

[29] A. Furui, T. Akiyama, and T. Tsuji, "A time-series scale mixture model of EEG with a hidden Markov structure for epileptic seizure detection," in *Proc. 43rd Annu. Int. Conf. IEEE Eng. Med. Biol. Soc. (EMBC)*, Nov. 2021, pp. 5832–5836.

[30] X. Hu, S. Yuan, F. Xu, Y. Leng, K. Yuan, and Q. Yuan, "Scalp EEG classification using deep bi-LSTM network for seizure detection," *Comput. Biol. Med.*, vol. 124, Sep. 2020, Art. no. 103919.

[31] T. Tsuji, N. Bu, O. Fukuda, and M. Kaneko, "A recurrent log-linearized Gaussian mixture network," *IEEE Trans. Neural Netw.*, vol. 14, no. 2, pp. 304–316, Mar. 2003.

[32] M. Hatamoto, A. Furui, K. Ogawa, and T. Tsuji, "Sleep EEG analysis based on a scale mixture model and its application to sleep spindle detection," in *Proc. IEEE/SICE Int. Symp. Syst. Integr. (SII)*, Jan. 2022, pp. 887–892.

[33] S. Fukuda, A. Furui, M. G. Machizawa, and T. Tsuji, "Stochastic fluctuation in EEG evaluated via scale mixture model for decoding emotional valence," in *Proc. IEEE/SICE Int. Symp. Syst. Integr. (SII)*, vol. 9, Jan. 2024, pp. 567–572.

[34] W. De Clercq, A. Vergult, B. Vanrumste, W. Van Paesschen, and S. Van Huffel, "Canonical correlation analysis applied to remove muscle artifacts from the electroencephalogram," *IEEE Trans. Biomed. Eng.*, vol. 53, no. 12, pp. 2583–2587, Nov. 2006.

[35] A. Vergult, W. De Clercq, A. Palmini, B. Vanrumste, P. Dupont, S. Van Huffel, and W. Van Paesschen, "Improving the interpretation of ictal scalp EEG: BSS–CCA algorithm for muscle artifact removal," *Epilepsia*, vol. 48, no. 5, pp. 950–958, Mar. 2007.

[36] D. Cosandier-Rimélé, F. Bartolomei, I. Merlet, P. Chauvel, and F. Wendling, "Recording of fast activity at the onset of partial seizures: Depth EEG vs. scalp EEG," *NeuroImage*, vol. 59, no. 4, pp. 3474–3487, Feb. 2012.

[37] T. Akiyama, B. McCoy, C. Y. Go, A. Ochi, I. M. Elliott, M. Akiyama, E. J. Donner, S. K. Weiss, O. C. Snead, J. T. Rutka, J. M. Drake, and H. Otsubo, "Focal resection of fast ripples on extraoperative intracranial EEG improves seizure outcome in pediatric epilepsy," *Epilepsia*, vol. 52, no. 10, pp. 1802–1811, Oct. 2011.

[38] J. A. Bilmes, "A gentle tutorial of the EM algorithm and its application to parameter estimation for Gaussian mixture and hidden Markov models," *Int. Comput. Sci. Inst.*, vol. 4, p. 126, Jan. 1998.

[39] C. M. Bishop, *Pattern Recognition and Machine Learning*. New York, NY, USA: Springer, 2006.

[40] V. Shah, M. Golmohammadi, S. Ziyabari, E. Von Weltin, I. Obeid, and J. Picone, "Optimizing channel selection for seizure detection," in *Proc. IEEE Signal Process. Med. Biol. Symp.*, Dec. 2017, pp. 1–5.

[41] L. Wang, X. Long, J. B. A. M. Arends, and R. M. Aarts, "EEG analysis of seizure patterns using visibility graphs for detection of generalized seizures," *J. Neurosci. Methods*, vol. 290, pp. 85–94, Oct. 2017.

[42] P. J. Werbos, "Backpropagation through time: What it does and how to do it," *Proc. IEEE*, vol. 78, no. 10, pp. 1550–1560, Oct. 1990.

[43] T. Tsuji, O. Fukuda, H. Ichinobe, and M. Kaneko, "A log-linearized Gaussian mixture network and its application to EEG pattern classification," *IEEE Trans. Syst., Man Cybern., C, Appl. Rev.*, vol. 29, no. 1, pp. 60–72, Feb. 1999.

[44] E. E. M. Reus, G. H. Visser, and F. M. E. Cox, "Using sampled visual EEG review in combination with automated detection software at the EMU," *Seizure*, vol. 80, pp. 96–99, Aug. 2020.

[45] J. Hughes, *EEG in Clinical Practice*. Boston, MA, USA: Butterworth-Heinemann, 1994.

[46] A. H. Mooij, B. Frauscher, J. Gotman, and G. J. M. Huiskamp, "A skew-based method for identifying intracranial EEG channels with epileptic activity without detecting spikes, ripples, or fast ripples," *Clin. Neurophysiol.*, vol. 131, no. 1, pp. 183–192, Jan. 2020.

AKIRA FURUI (Member, IEEE) received the B.Eng., M.Eng., and Ph.D. degrees from Hiroshima University, Hiroshima, Japan, in 2016, 2018, and 2019, respectively. From 2018 to 2019, he was a Research Fellow with Japan Society for the Promotion of Science. He is currently an Associate Professor with the Informatics and Data Science Program, Graduate School of Advanced Science and Engineering, Hiroshima University. His research interests include biosignal processing, human interface, machine learning, medical image processing, and stochastic modeling.

RYOTA ONISHI received the B.E. and M.E. degrees from Hiroshima University, Hiroshima, Japan, in 2019 and 2021, respectively.

TOMOYUKI AKIYAMA received the M.D. and Ph.D. degrees from Okayama University, Okayama, Japan, in 1995 and 1999, respectively. He is currently an Associate Professor with the Department of Pediatric Neurology, Okayama University Hospital.

TOSHIO TSUJI (Life Member, IEEE) was born in Kyoto, Japan, in December 1959. He received the B.E. degree in industrial engineering and the M.E. and D.Eng. degrees in systems engineering from Hiroshima University, Hiroshima, Japan, in 1982, 1985, and 1989, respectively. From 1992 to 1993, he was a Visiting Professor with the University of Genoa, Italy. Since 2002, he has been a Full Professor with Hiroshima University. His research interests include human science with a focus on cybernetics, medical electronics, computational neural sciences, and particularly biological Kansei modeling. He has received 54 academic awards, including the IEEE King-Sun Fu Memorial Best Transactions Paper Award, in 2003 and the Good Design Award, Japan, in 2006.

• • •